JOURNAL OF TISSUE ENGINEERING AND REGENERATIVE MEDICINE
J Tissue Eng Regen Med (2015)
Published online in Wiley Online Library (wileyonlinelibrary.com) **DOI:** 10.1002/term.1994

REVIEW

An insight into morphometric descriptors of cell shape that pertain to regenerative medicine

Joana Lobo, Eugene Yong-Shun See, Manus Biggs and Abhay Pandit*
Network of Excellence for Functional Biomaterials (NFB), National University of Ireland, Galway, Ireland

Abstract

Cellular morphology has recently been indicated as a powerful indicator of cellular function. The analysis of cell shape has evolved from rudimentary forms of microscopic visual inspection to more advanced methodologies that utilize high-resolution microscopy coupled with sophisticated computer hardware and software for data analysis. Despite this progress, there is still a lack of standardization in quantification of morphometric parameters. In addition, uncertainty remains as to which methodologies and parameters of cell morphology will yield meaningful data, which methods should be utilized to categorize cell shape, and the extent of reliability of measurements and the interpretation of the resulting analysis. A large range of descriptors has been employed to objectively assess the cellular morphology in two-dimensional and three-dimensional domains. Intuitively, simple and applicable morphometric descriptors are preferable and standardized protocols for cell shape analysis can be achieved with the help of computerized tools. In this review, cellular morphology is discussed as a descriptor of cellular function and the current morphometric parameters that are used quantitatively in two- and three-dimensional environments are described. Furthermore, the current problems associated with these morphometric measurements are addressed. Copyright © 2015 John Wiley & Sons, Ltd.

Received 21 May 2013; Revised 25 August 2014; Accepted 9 December 2014

Keywords morphometry; image analysis; quantitative microscopy

1. Introduction

Cell shape has long been considered an important indicator of the events occurring in the cellular microenvironment and is associated with unique specificity in the cells of specific organs and tissues (e.g. tenocytes elongate in the direction of loading to impart mechanical strength and neurons generate multiple branching and interconnecting dendrites to facilitate complex cellular networking) van Pelt *et al*., 2004.

Cell morphology is a dynamic process with considerable implications in tissue engineering and regenerative medicine. Attempts to regulate cellular morphology through external cues and biomimetic solutions are emerging as important methodologies in biomedical engineering and medicine. In particular biochemical and physico-mechanical modulation has become integrated into biomaterial and tissue engineering design through molecular biofunctionalization (Zychowicz *et al*., 2012; Satyam *et al*., 2014) and tailored rigidity/topography (Engler *et al*., 2006; Dalby *et al*., 2007c; Oh *et al*., 2009) and rigidity.

Cellular morphology is a function of the dynamic interactions and the balance between forces occurring between the cytoskeleton, cell membrane, and adhesion complexes that interface with the extracellular matrix, often via the actions of regulatory signal transduction systems (Watson, 1991). The study of biological and cellular shapes is indeed a challenge, and a lack of standardized procedure restricts or prevents comparative studies. Traditional approaches have relied on visual observation, subjective assessment, and qualitative analysis of images. The concept of morphometric assessment of cell shape was introduced in the early 1900s, with studies on cell volume (Jacob, 1925) and reports on nuclear size (Heiberg and Kemp, 1929) soon following. However, it was not until the 1980s that cellular morphometric

Correspondence to: Abhay. Pandit, Network of Excellence for Functional Biomaterials (NFB), National University of Ireland, Galway, Ireland. E-mail: abhay.pandit@nuiglaway.ie

analysis tools started to be used to assist researchers with the identification of cellular phenotypic variations that documented a change in the cellular environment. Quantitative geometrical analyses of cell structure, as well as subcellular components, were established using morphometric descriptors and tools. As a consequence, the reliability of image-based cellular studies increased as researchers attempted to translate the qualitative differences observed microscopically to quantitative measurements to establish an objective analysis of cell shape based on numerical results (Pasqualato *et al*., 2012).

Suitable objective parameters have since been defined to express the relevant geometrical features of the cell. Each of these quantitative features for the analysis of cell shape (also called 'morphometric parameters' or 'descriptors') measures and characterizes a certain cellular attribute. Cellular shape descriptors need to be straightforward while allowing for the extraction of information that is biologically meaningful, easy to interpret and allows direct morphological correlation with representative images. A good descriptor should also work well across a range of cell types, culture conditions and imaging methods (Pincus and Theriot, 2007). In addition, it is important that these descriptors are also able to reveal information about cell shape that is not easily discernible by cursory visual inspection (Soltys *et al*., 2001).

Quantitative analysis of cellular and subcellular structures is a powerful tool in biology and tissue engineering. It allows whole-cell comparison between diverse cell types (Thurner *et al*., 2005) and facilitates morphological characterization of subcellular structures, (i.e. focal adhesions and cell nuclei) (Nandakumar *et al*., 2012). Importantly cellular morphology may be characterized over time, via live-cell imaging, to observe morphological changes associated with cellular spreading and motility or in response to external stimuli (Xiong and Iglesias, 2010). Critically, cell shape analysis can also help to analyse pathologies across a range of tissue types (True, 1996), and has been used to assess the cellular transition towards a drug-resistant phenotype (Pasqualato *et al*., 2012) and to analyse the cellular components of artificial organs in cytotoxicity and biocompatibility testing (den Braber *et al*., 1996; Metzler *et al*., 1999, 2000).

Importantly, cell morphology can also be employed to evaluate cellular differentiation (Wan *et al*., 2010) and correlate cell shape with cell function (Watson, 1991; Costa *et al*., 2002). This shape–function paradigm, aims to correlate the cell shape to biological processes such as proliferation (Chen *et al*., 1997), differentiation (Watt *et al*., 1988; Roskelley *et al*., 1994), cell migration, behaviour, motility, and growth dynamics (Keren *et al*., 2008; Xiong and Iglesias, 2010). Shape quantification can also be used to analyse cell-to-cell interactions to assess cellular communication and juxtacrine signalling (den Braber *et al*., 1996). One of the most clinically significant applications of cell shape analysis is in oncological research, and morphometric descriptors have been used to predict behaviour, malignancy, and disease outcome of cancer cells.

This review gives an overview of the morphometric descriptors that have been used in cellular and bioengineering research for cell shape analysis. Shape descriptors are described and the significance of these descriptors discussed along with the problems associated with their use. Finally, an outlook of the future of morphometric analysis is presented. Image acquisition, as well as the related processing techniques, will not be discussed in this article as these aspects are already extensively covered by others (Zhang and Lu 2004; Chen *et al*., 2011, 2012; Eliceiri *et al*., 2012).

2. Morphometric descriptors

Morphological parameters can be categorized according to the major features described (Lepekhin *et al*., 2001), the type of quantitative information given, or the complexity of the parameter. In this section, morphometric descriptors will be categorised by dimensionality—two-dimensional (2D) or three-dimensional (3D)—and the cellular region or structure being evaluated (the entire cell, nucleus, or other secondary organelles). An overview of 2D morphometric descriptors is illustrated in Figure 1.

2.1. 2D cell morphometry

Two-dimensional cell morphometry of histological or cytological image analysis has historically been a balance of interpretation and objective knowledge dependent on visual recognition of changes in cellular and subcellular morphology and knowledge of what those patterns mean with respect to tissue injury (Boyce *et al*., 2010). Quantitative histopathology and cytology has become a core component of the diagnostic and scientific process in pathology, biomaterials, and tissue engineering research, being employed in both *in vitro* and *in vivo* studies to assess the cellular response in terms of morphological descriptors.

2.1.1. Simple descriptors

Simple description parameters are employed in the description of general features of cellular morphology, using one quantitative variable that can be assessed with basic image analysis software. Within this category, parameters can be divided into geometrical features and shape features (Chen *et al*., 2012). These descriptors are commonly employed in cytology to characterize closed contour shapes (i.e. the cell area) (Biggs *et al*., 2007a) and to characterize subcellular features, including nuclear volume (Cassidy *et al*., 2014) and focal adhesion area (Biggs *et al*., 2009a, 2009b). Simple descriptors are useful in cell biology as an easy method to assess complex cellular processes; for example, nuclear elongation has been implemented in differential gene expression (Dalby *et al*., 2007a, 2007b), and focal adhesion area can be an indicator of cellular adhesion (Schiller and Fassler, 2013).

DOI: 10.1002/term

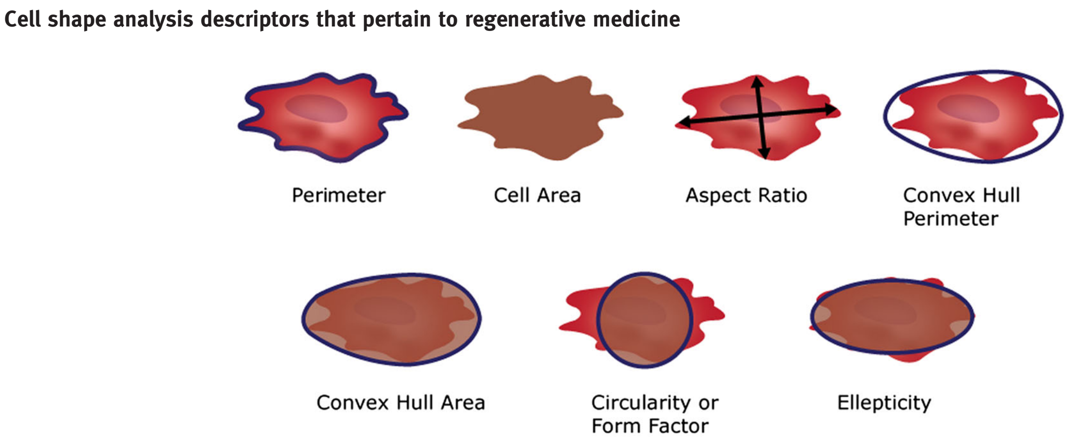

Figure 1. Schematic illustration of two-dimensional morphometric cell descriptors. More descriptors and details of formulae are listed in Table 1

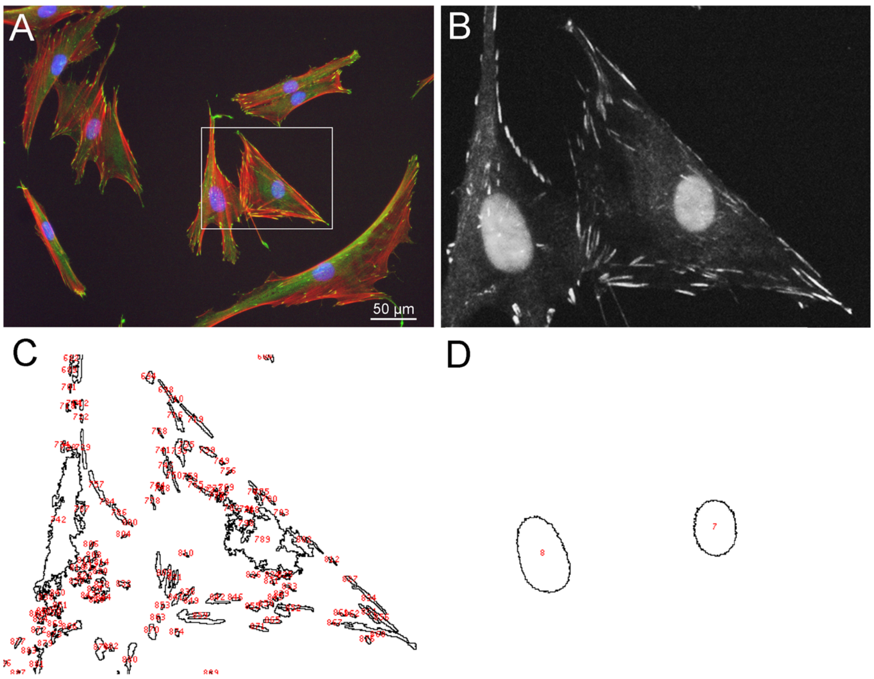

Figure 2. Focal adhesion and nuclear morphometry of epifluorescent images. (A) Human dermal fibroblast are tri-labelled for F-actin (red) the focal adhesion protein vinculin (green) and the nucleus (blue). (B) High magnification two-channel image of boxed area. (C,D) Threshold identification and outline images of (C) focal adhesion and (D) nuclei

Nuclear and focal adhesion subcellular analysis of fluorescent images is outlined in Figure 2 and all the mathematical expressions of the geometrical and shape features presented in this section are summarized in Table 1.

Geometric features describe basic morphometric variables, i.e. perimeter, area, and cellular radii. As a point of reference, perimeter is calculated as the sum of the individual distances between adjacent points of a contour, while area refers to the region surrounded by that closed contour, meaning the number of pixels within that region (Lepekhin *et al*., 2001) Similarly, radii are obtained from the projection of cell area and have significance only if the cell is circular (Chen *et al*., 2012). These descriptors are frequently used to assess cellular spreading, in particular useful for assessing adhesion and at the tissue implant interface *in vitro* (Biggs *et al*., 2007b; Massia and Hubbell, 1991). Cell spreading can be employed as a *de facto* assay of material cytocompatibility. Furthermore, simple analysis of cell area can be employed in biomaterials studies to study real-time loss of cellular adhesion, such as with dynamic photoresponsive and thermoresponsive polymeric systems (Oh *et al*., 2014).

These geometric features can subsequently be utilized as shape descriptors. The most commonly used of which is form factor (Berezin *et al*., 1997; Soll *et al*., 1988; Lepekhin *et al*., 2001) also called circularity (Schneider *et al*., 2012) or compactness (Metzler *et al*., 2000), being a ratio between the area and the square of the perimeter, as shown in Table 1. Sometimes it is inappropriately used with its reciprocal, roundness (Behnam-Motlagh *et al*., 2000). Both descriptors are rotation invariant and size-independent indicators of the degree of cell circularity and shape

Table 1. Mathematical formulae of the most commonly used two-dimensional morphometric descriptors for cell shape analysis

Shape Descriptor	*Formula*	*Notes*	*References*
Simple Descriptors			
Geometrical Features			
Perimeter (P)	$\sum_{i=0}^{n-1}\sqrt{(x_i - x_{i+1})^2 + (y_i - y_{i+1})^2}$	Sum of the individual distances between adjacent points of the contour with length *n*	Lepekhin *et al*. (2001)
Area (A)	$\left\lvert \frac{1}{2}\sum_{i=0}^{n-1}(x_i \cdot y_{i+1} - x_{i+1} \cdot y_i) \right\rvert$	Region surrounded by the closed contour with length *n*	Lepekhin *et al*. (2001)
Shape Features			
Circularity or form factor	$\frac{4\pi \cdot \mathrm{Area}}{\mathrm{Perimeter}^2}$	Value 1 is a perfect circle and less than 1 an oblong shape.	Schneider *et al*. (2012)
Roundness	$\frac{\mathrm{Perimeter}^2}{4\pi \cdot \mathrm{Area}}$	The reciprocal of circularity	Behnam-Motlagh *et al*. (2000)
Aspect ratio	$\frac{\mathrm{Major\ \ Axis\ \ Length}}{\mathrm{Minor\ \ Axis\ \ Length}}$	Value 1 is a circle	Schneider *et al*. (2012)
Eccentricity	$\sqrt{1 - \left(\frac{\mathrm{Minor\ \ Axis\ \ Length}}{\mathrm{Major\ \ Axis\ \ Length}}\right)^2}$	Values between 0, are a perfect circle, and 1, when shape degenerates into a straight line	Bray *et al*. (2010)
Ellipticity	$\frac{\mathrm{Form\ \ Factor}}{\mathrm{Eccentricity}}$	Value 1 is a regular ellipse	Nafe *et al*. (2001)
Solidity	$\frac{\mathrm{Cell\ \ Area}}{\mathrm{Convex\ \ Hull\ \ Area}}$	Value 1 means a solid object and lower values irregular boundaries or holes.	Soltys *et al*. (2005)
Convexity factor PERBAS	$\frac{\mathrm{Convex\ \ Hull\ \ Perimeter}}{\mathrm{Cell\ \ Perimeter}}$	Perimeter ratio before and after smoothing: value 1 is a square and lower values mean an enlargement of cell surface area	Payne *et al*. (1989)
Spreading index	$\frac{\pi \cdot \mathrm{Convex\ \ Hull\ \ Perimeter}^2}{4 \cdot \mathrm{Convex\ \ Hull\ \ Area}}$	Larger values indicate more elongated structures	Rocchi *et al*. (2007)
Branching descriptors			
Number of branching points	Number of primary, secondary and tertiary branch points	Cell body primary projections and secondary branches, originated within that projection with a length greater than 5 mm, are counted	Kumar *et al*. (2011)
Branching density	$\frac{\mathrm{Area\ of\ Skelotinized\ Image}}{\mathrm{Convex\ Hull\ Area}}$	High density may indicate increased number of connections	Soltys *et al*. (2005)
Ramification factor	$\frac{\mathrm{Number\ of\ Terminal\ Segments}}{\mathrm{Number\ of\ Terminal\ Processes}}$	Ramified structures have higher values	Soltys *et al*. (2005)
Branch or path length	Total length of the path of the process from the dendritic root to the terminal tip	May be affected by the cutting plane applied	Rocchi *et al*. (2007)
Radial distance	Minimal length from the dendritic root to the terminal tip.	The difference between path length and radial distance can assess branch straightness.	Rocchi *et al*. (2007)
Branching angle	Angle measured between branches	Requires circular statistics	Rocchi *et al*. (2007)
Fractal geometry			
Fractal dimension (D)	$\mathrm{D} = \log\ \mathrm{N}\ \log\ \varepsilon$	N is related to the shape's detail changes, and ε is the size or scale considered	Smith *et al*. (1996)
Lacunarity (LAC)	$\mathrm{LAC} = \mathrm{CV}^2_{\varepsilon,g} = \left(\frac{\sigma_{\varepsilon,g}}{\mu_{\varepsilon,g}}\right)^2$	CV is the coefficient of variation of pixels for each grid position g and scale ε, obtained using the standard deviation σ and mean μ	Smith *et al*. (1996)
Other descriptors			
Bending energy	$\mathrm{B} = \frac{1}{\mathrm{P}}\int_0^{\mathrm{P}} \mathrm{K(p)}^2 \mathrm{dp}$ $\mathrm{K(p)} = \frac{\mathrm{d}\theta}{\mathrm{dp}}$	K is the curvature function defined as the rate of change in tangent direction θ of the contour, as a function of the arc length p. B is normalized by total curve length P	Bowie and Young (1977); Pasqualato *et al*. (2012)

DOI: 10.1002/term

irregularities. A value of '1' corresponds to a perfect circle while values lower than '1' for the form factor and a value higher than 1 for the roundness reveal an oblong shape with protrusions exposing the complexity of cell boundary. Similarly, cell area factor (CAF) is obtained by multiplying cell area by roundness, resulting in an area feature with a circularity assessment.

Recent studies into tissue regeneration have employed circularity to determine shape changes associated with apoptosis (Helmy and Azim, 2012), and age-related degeneration (Jiang *et al*., 2014). Here it was noted that cells adopted a rounded morphology when undergoing apoptosis.

In tissue engineering, curvature factors are also useful for expressing the space-filling capacity of the cell and in assessing the occurrence of concave or convex irregularities which may effect accurate analysis of total cell area. The concavity factor PCAF (per cent concave area fraction), as well as solidity, is calculated from a ratio involving the area of the cell and of its convex hull (Soltys *et al*., 2001). Although these formulae are different, both factors can be used as a measure of the density of a cell or a cellular construct. A solidity of '1' corresponds to a solid object while lower values reveal irregular boundaries or concavities. A recent study by Booth-Gauthier *et al*. (2013) employed solidity in the analysis of cellular morphology and motility on microscale structures. Here they reported an increase in nuclear solidity in Hutchinson–Gilford progeria syndrome (HGPS) cells, a premature aging disorder (Booth-Gauthier *et al*., 2013). The authors concluded that the nucleus of HGPS cells was significantly less compliant than control fibroblast cells. The convexity factor PERBAS (perimeter ratio before and after smoothing), also known only as convexity, is obtained by dividing the perimeter of the contour's convex hull by cell perimeter, indicating the relative deviation of cell shape from a convex object. Decreasing convexity indicates an enlargement of cell surface area in comparison to the space occupied by the cell (Payne *et al*., 1989; Soltys *et al*., 2001).

The spreading index measures the degree of roundness of the convex hull, reflecting cellular spreading and polarization. A larger value of this index will indicate more elongated structures (Kawa *et al*., 1998). For example, this index has been used to characterize the morphology of growing spinal motor neurons (Stahlhut *et al*., 1997).

With respect to cellular polarity and isotropy the geometric aspect or axial ratio of the cell is given by the direct ratio of the cellular major axis to the minor axis (Schneider *et al*., 2012). Studies utilizing bioreactor systems which apply shear stress often employ analysis of the cellular aspect ratio or cellular elongation to assess the cellular morphological response to fluid flow. Liu *et al*. (2010) utilized this technique to quantify changes in morphological anisotropy in response to continuous flows. Here it was noted that in rat osteoblasts the aspect ratio is increased and circularity is significantly decreased with flow-induced stresses greater than 1.2 Pa (Liu *et al*., 2010).

Similarly, eccentricity is defined as a ratio between the major and minor axis of the ellipse that contains the cell. Although, eccentricity is commonly used for nuclear morphology (Bray *et al*., 2010), both descriptors can assess cell polarity by distinguishing between non-elongated and elongated shapes. Correlations between perturbed nuclear morphology and certain disease states are well documented; most notably, many cancers are diagnosed and the stage identified by changes to, or graded increases in nuclear size (Pearson, 1986; Chow *et al*., 2012).

Eccentricity is a derivative of values between '0', a perfect circle, and '1', when the shape degenerates into a straight line. Following, the ellipticity or ellipse shape factor is obtained by dividing the cell form factor by the form factor of a perfect ellipse to measure the deviation from an elliptical shape. Hence, this parameter is '1' for a regular ellipse (Nafe *et al*., 2001). Bray *et al*. (2010) used eccentricity to analyse cellular and nuclear morphological responses in cardiomyocytes cultured on micro-contact printed protein arrays. It was concluded that cardiomyocytes cultured in anisotropic tissues possess a higher nuclear eccentricity and that these changes likely resulted from direct mechanotransduction pathways [i.e. tensional forces being translated from the extracellular matrix (ECM) to the nucleus through the cytoskeleton].

Resistance to deformation can also be described by the bending energy descriptor, derived by the integrated sum of squared curvature values to assess variability of the complex and irregular cell contours. This corresponds to the amount of energy necessary to return that shape to its lowest energetic state. For example, a straight line would have zero energy whereas a more complex contour would hold higher bending energy values (Costa *et al*., 2002; Pasqualato *et al*., 2012). Bowie and Young (1977) proved that the shape with minimal average bending energy was a circle with the same perimeter as the shape of interest. A recent study by López *et al*. (2012) explored the role of sphingolipid synthesis on bending energy in erythrocytes. The research concluded that bending energy may play a crucial role in translating external stresses and that this is strongly regulated by the synthesis of sphingolipids. A multiscale version of this descriptor has also been described and this helps in describing the evolution of 'shape energy' along a smoothing process (Costa *et al*., 2002). Bending energy has been used to describe both cellular and subcellular morphology, particularly in relation to lipid bilayer-enclosed structures (Sackmann, 1994).

Pursuit of a complete tensegrity theory and the observation that cytoskeletal development is adhesion mediated has led to the concept that mechanical signals are transferred from the ECM, across anchoring focal adhesions via the molecular filament networks that form the cytoskeleton to the nucleus, essentially forming a single physical lattice extending from the ECM to the nucleoskeletal network. This is in agreement with Forgacs' (1995) percolation theory whereby he describes the ECM as the spiders web and changes in stress/strain of the web will be relayed to the spiders body (nucleus) via its legs (cytoskeleton). In this sense, tensegrity is

DOI: 10.1002/term

simply a specialized percolation network with both theories agreeing that an interconnected cytoskeletal network is required for the transmittal of mechanical signals, resulting in nuclear deformation.

The nuclear area factor (NAF) aims to characterize nuclear shape changes and is derived from the product of nuclear area and nuclear roundness. This parameter is used as an indicator of apoptotic processes characterized usually by low values of NAF owing to small and round nuclei (Daniel and DeCoster, 2004). Another area-derived parameter for the nuclei is the coefficient of variation of nuclear area (NACV), given by the ratio between the standard deviation of nuclear area and the mean nuclear area. This expresses the variation in nuclear size (Nagashima *et al*., 1998). To assess the smoothness of a nuclear contour, the mean nuclear regularity factor is used, having a value of '1' for smooth borders and less than '1' for irregular ones (Nativ *et al*., 1995). Details of nuclear features have been summarized in Table 2 and illustrated in Figure 3.

Simple descriptors are often used in tissue engineering to describe cellular morphometric responses to physico-mechanical cues, particularly to asses cellular alignment and spreading in response to topography (Cassidy *et al*., 2014), mechanical loading (Mauri *et al*., 2013), and substrate rigidity (Lautscham *et al*., 2014). Cellular spreading has been utilized extensively as an indicator of biomaterial cytocompatibility (Kantawong *et al*., 2009; Binulal *et al*., 2010) with many studies indicating enhanced function with increased cellular area. In particular nanotopography has emerged as a potent regulator of cellular spreading and differential function (Dalby *et al*., 2007c). Conversely, inducing cellular elongation through topographical cues or the application of shear or tensional forces has been associated with enhanced differential function in tenocyte (Tong *et al*., 2012), endothelial (McKee *et al*., 2012), and smooth muscle cells (Rayatpisheh *et al*., 2014).

2.1.2. Branching descriptors

Branching descriptors are used extensively for characterization of neuron morphology by quantifying complexity and ramification patterns of neural cells. In neurology, there are a particularly large number of metrical parameters that can be used, especially because of the vast multiplicity of morphological shapes of neural cells. Basic parameters include, for example, the number of branching points, which simply count the number of projections from the cell body (primary branch points) and branches originating within that projection with a length greater than 5 μm (secondary and tertiary branch points) (Yao *et al*., 2009; Kumar *et al*., 2011). The ramification factor is the ratio between the number of terminal segments and the number of primary processes. This value is higher for ramified structures. To measure these factors, it is necessary to do a skeletonization that reduces the neuronal tree to a skeleton of segments connecting branching points and terminal segments (Hines and Carnevale, 2001). Branching density is the area of the skeletonized cell divided by the area of the convex hull (Soltys *et al*., 2001, 2005). Other branching descriptors extracted from the skeletonized neuron include the Path Length (total length of the path of the process from the dendritic root to the terminal point), the radial distances (minimal length from the centre of cell body to the terminal processes), and the bifurcation or branching angles. In addition, the difference between path length and radial distance can be used to assess branch straightness (Rocchi *et al*., 2007). A study by Payne *et al*. (2014) recently described a method to evaluate neurite orientation distributions suitable for objectively assessing the anisotropy induced by carbon nanotubes arrayed in parallel bundles over gold surfaces. Similarly, in the field of drug screening and biomaterials there is considerable interest in compounds that modulate the anisotropy of the cytoskeleton, whether cellular microtubules, intermediate filaments, or actin filaments which have been shown in many studies to become organized in response to growth factors (Moustakas and Stournaras, 1999), drugs (Muller *et al*., 2013), surface topography (Biggs *et al*., 2009a, 2009b), and material rigidity.

The generation of neuronal networks and subsequent neurite extension and branching is a reliable indicator of differential neuronal function and the analysis of neurite branching is extensively employed in biomaterials and tissue engineering to assess neural induction and phenotype maintenance *in vitro*. In particular quantification of neurite branching has been recently employed to assess the neuron response to soluble signalling factors (Spillane *et al*., 2012; Wu *et al*., 2012; Howard *et al*., 2013), the matrix microenvironment (Deister *et al*., 2007; Kothapalli and Kamm, 2013; Kraskiewicz *et al*., 2013), and external electrical stimulation (Wood and Willits, 2009; Chang *et al*., 2013; Royo-Gascon *et al*., 2013). These 2D branching descriptors are illustrated in Figure 3.

Table 2. Mathematical formulae of the most used two-dimensional morphometric descriptors for nuclear shape analysis

Shape descriptor	*Formula*	*Notes*	*References*
2D nuclear morphometry			
Nuclear area factor (NAF)	Nuclear Area · Roundness	Low values mean small and round nuclei	Daniel and DeCoster (2004)
Coefficient of variation of nuclear area (NACV)	$\frac{\sigma_{NA}}{\text{Mean Nuclear Area}} \cdot 100$	σ_{NA} is the standard deviation of nuclear area	Nagashima *et al*. (1998)
Mean nuclear regularity factor (MNRF)	$\frac{\text{Nuclear Area}}{\pi/4 \cdot \text{Max Diameter} \cdot \text{Min Diameter}}$	A value of 1 indicates smooth borders and less than 1 indicates irregular borders	Nativ *et al*. (1995)
Nuclear elongation factor or LS ratio (MNEF)	$\frac{\text{Maximum Diameter}}{\text{Minimum Diameter}}$	The same as the nuclear aspect ratio	Nativ *et al*. (1995); Nagashima *et al*. (1998)

DOI: 10.1002/term

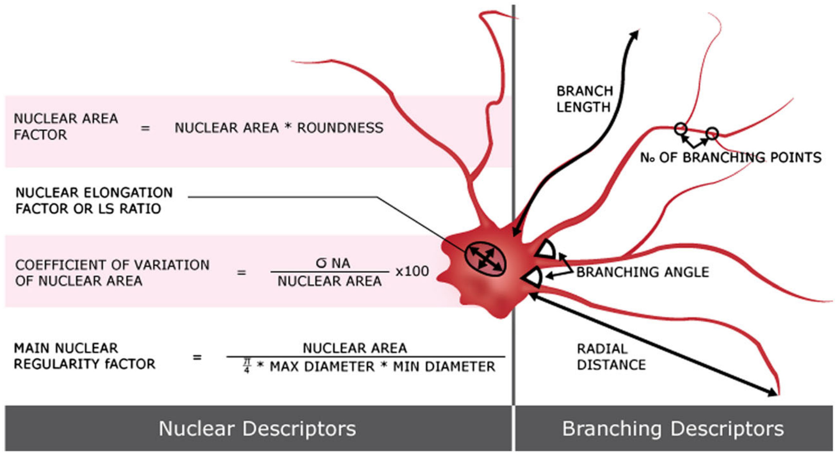

Figure 3. Schematic illustration of nuclear morphometric parameters (left) and two-dimensional branching descriptors (right). NA, nuclear area

2.1.3. Fractal geometry

Although fractal-related descriptors require more computational effort than the simple morphological descriptors identified above, fractal geometry, introduced in 1982 by Mandelbrot, is also helpful for neuromorphometric studies (Bernard *et al*., 2001; Costa *et al*., 2002). A fractal is a self-similar structure or, in other words, an object that retains its shape proprieties independent of the scale of measurement. Fractal dimensions (D) are quantitative measures of this self-similarity. These measures have been reported as suitable descriptors for cell morphology as they identify small variations of the space-filling capacity of cell shape and indicate how a rugged boundary is distributed over a void space (Soltys *et al*., 2005). Thus, fractal dimensions are objective measures of cell border roughness, cell shape complexity and the amount of cell branching. In view of this, the fractal dimension or D-value increases with the complexity of the contour, where a D of '1' represents a straight line. There are several processes that can be used to obtain fractal dimensions and are divided into length-based or mass-based methodologies, with length-related measures used for the assessment of cellular morphology *in vitro*. When using length-based methodologies, lengths or distances between points on the contour are measured to obtain the capacity dimension (D_c) using a trace, dilation or a box-counting method. Mass-related methodologies count the border pixels within sampling regions (usually discs of several diameters) as a function of their size, subsequently estimating the 'sandbox' or cumulative mass, or mass-radius dimension (D_{MR}) (Smith *et al*., 1996).

Fractal analysis has proved particularly useful with regard to electron microscopy for the objective investigation of fine cytoplasmic structures and the organization of various types of chromatin, nuclear components, and other subcellular organelles, both in normal and pathological tissues and in cell cultures (Losa, 2012). As with analysis of cellular circularity, fractal analysis has also been employed to correlate ultra-structural changes in cell surface and nuclear inter(eu)chromatin with the early phases of apoptosis in human breast cancer cells. These ultrastructural change were evident well before the detection of conventional cell markers, which were only measurable during the active phases of apoptosis (Losa *et al*., 1998).

In histology and cytology, microscopic analysis through fractal morphometry of cell nuclei and has greatly improved the understanding of cell behaviour and the diagnosis and prognosis of various diseases (Muniandy and Stanslas, 2008). In particular, quantification of nuclear chromatin organization by fractal morphometry is used to evaluate the degree of malignancy in histological sections from breast tissue (Einstein *et al*., 1998) and in aspiration cytology smears of cervical lesions (Ohri *et al*., 2004). Among many other applications, fractal dimensions have been used to assess the developmental stages of oligodendrocytes (Bernard *et al*., 2001), characterize normal and malignant hepatocytes (Boæovi *et al*., 2000), and microglial cells (Soltys *et al*., 2005).

Fractal dimensions are insensitive to some shape patterns and therefore cannot be used as unique descriptors (Smith *et al*., 1996; Soltys *et al*., 2001). To overcome this, D can be combined with another morphometric descriptor, lacunarity (LAC or λ) (Smith *et al*., 1996; Soltys *et al*., 2005), which is used to assess structural variance or non-uniformity of the cell (Smith *et al*., 1996). For equivalent fractal dimensions, cells with the most irregular shape have the highest lacunarity (Soltys *et al*., 2005; Rocchi *et al*., 2007).

Fractal dimension analysis is also particularly interesting as a morphometric descriptor in tissue engineering for the analysis of 3D networks *in vivo* (Leslie-Barbick *et al*., 2011; Lang *et al*., 2012) and tissue engineered constructs to assess interconnectivity, porosity, and morphology (Guarino *et al*., 2010). Importantly, fractal dimension analysis lends itself very well to the analysis of

DOI: 10.1002/term

computerised topography and scanning electron microscopy (SEM) micrographs.

2.2. 3D morphometry

Three-dimensional fluorescence imaging is fast becoming important for accessing disease progression in clinical trials. Often, a 3D volume block is constructed from point-by-point or at best plane-by-plane scanning of the specimen. Tools for 3D imaging, coupled with high-powered computing have brought a new perspective to the analysis of cellular morphology. It is widely accepted that confocal laser scanning microscopy (CLSM) and other derivative techniques (e.g. fluorescence resonance energy transfer (FRET)) are currently the state-of-the-art image technologies in 3D microscopy, although electron (Bonnet *et al*., 1996) or two-photon microscopy (Débarre *et al*., 2009) can also be useful in determining cell density as well as temporal and spatial cellular, or subcellular distributions (Kim *et al*., 2011).

Building on principals of 2D imaging techniques, a 3D perspective of cell morphometry integrates both surface area and volume computation. Calculating cellular or nuclear surface area requires computation of the approximated number of voxels within a given area that have at least one background voxel as a neighbour. Similarly, the volume of the cell or of its nucleus (Fujikawa *et al*., 1997) is given by the total number of voxels within the object adjusted by the appropriated spatial scale (Choi and Choi, 2007). A geometric model of cell volume can also be approached through infinite element-modelling processes (Walker *et al*., 2003).

Owing to the quality and high definition of cell images obtained through CLSM, it is used for many applications, including immunocytochemical detection of nuclear or other organelles as well as localization of specific proteins (Hevia *et al*., 2011). In addition to cell imaging capabilities, CLSM has opened a broad range of new image-related possibilities to solve biological questions (Ntziachristos, 2010) via 3D reconstruction (Luzzati *et al*., 2011). Critically, accurate quantification of cell volume is useful in many facets of regenerative medicine, including morphometric studies, physiological studies (Kiehl *et al*., 2011), or estimation of intracellular concentration of substances (Hevia *et al*., 2010). For example, a useful descriptor in 3D analysis of cell morphology is the NC (nucleus to cytoplasm) ratio or the ratio of the volume of the nucleus to the volume of the cell. This factor quantifies volumetric differences and volume changes in 3D, and has been used to assess the maturity of a cell (Nayar and Sundharam, 2003) or in the assessment of stages of cancer development (Walker *et al*., 2003). Song *et al*. (2013) recently employed the NC ratio technique to evaluate normal and apoptotic endothelia cells in CLSM-acquired images. Specifically, their results revealed that H_2O_2 can induce apoptosis in endothelial cells by regulating the activity of apoptosis-related biomolecules, including pro-apoptotic factors p53 and Bax, and anti-apoptotic factor Bcl-2. Furthermore, when compared with normal endothelial cells the apoptotic cells exhibited significant 3D nucleus-to-cytoplasm ratio variation (Song *et al*., 2013).

As with a 2D object, the form factor can also be extended to a 3D environment to obtain sphericity, a measure of how efficiently a given surface encloses a volume. In other words, it quantifies how closely the shape of the cellular or subcellular structure approaches to a perfect sphere—a hypothetical morphology with a sphericity of 1 (Nandakumar *et al*., 2011). Sphericity is frequently employed to assess modulations to the nuclear morphology associated with neoplastic progression as well as the cellular response to 3D scaffolds or external cellular stressors. A study by Baker *et al*. (2010) describes the use of a particle-tracking microrheology approach to investigate the interplay among intracellular mechanics, three-dimensional matrix stiffness, and transforming potential in a mammary epithelial cell cancer progression series. A further study by Khoshfetrat *et al*. (2008) examined the morphological effects of transforming growth factor beta on chondrocytes embedded within a collagen gel matrix. Based on the morphology-related variable of sphericity for individual cells, it was found that the presence of transforming growth factor (TGF) beta-1 caused a reduction in sphericity and an increase in the fraction of migrating chondrocytes (Khoshfetrat *et al*., 2008). Furthermore, both solidity (the ratio between convex surface area and surface area) and convexity (the ratio between volume and convex volume) can also be translated into to 3D descriptors following calculation of the 3D convex hull and have been employed in studies investigating HER2 antibody treatments in breast cancer (Emde *et al*., 2011), and in investigating the effect of neuroprotectin D1 signaling on microglial cells in laser-induced choroidal neovascularization, respectively (Sheets *et al*., 2013).

The 3D morphometric descriptors related to the shape of the individual cell along with their mathematical derivations are given below (Table 3). As 3D-features require laborious computational algorithms, only an overall approach to each descriptor is discussed.

2.3. Non-morphometric descriptors

As well as morphometric descriptors, quantitative analysis of non-geometric parameters can give information indirectly about cell morphology and function such as texture descriptors, pixel intensity, and contour temperature. One of the commonly used techniques to extract cell texture features is based on the grey level co-occurrence matrix (GLCM) (Losa and Castelli, 2005), and is a valuable mathematical method for quantification of cell and tissue textural properties, such as homogeneity, complexity and level of disorder. Recently, it was demonstrated by Pantic *et al*. (2013b,2013c) that this method is capable of evaluating fine structural changes in nuclear structure that are otherwise undetectable during standard microscopy analysis, and thus is useful for the identification of nuclear

DOI: 10.1002/term

Table 3. Mathematical formulae of the most common three-dimensional morphometric descriptors for cell and nucleus shape analysis

Shape descriptor	Formula	Notes	References
3D morphometry Surface area	$S = \sqrt{s(s-a)(s-b)(s-c)}$ $s = \frac{(a + b + c)}{2}$	a, b, c are the lengths of the sides of a triangle	Choi and Choi (2007)
Volume	Total number of voxels in the cell multiplied by voxel size	Can also be approached through infinite element modelling	Choi and Choi (2007)
Nucleus to cytoplasm ratio (NC ratio)	$\frac{\text{Nuclear Volume}}{\text{Cell Volume}}$	Usually decreases as cell matures	Nayar and Sundharam (2003)
Sphericity or three-dimensional (3D) form factor	$\frac{36\pi \cdot \text{Volume}^2}{\text{Surface Area}^3}$	A perfect sphere has a sphericity of 1	Choi and Choi (2007)

abnormalities, tumour grading, and diagnosis (Kim *et al*., 2010; Liautaud-Roger *et al*., 1992; van Velthoven *et al*., 1995). Importantly, combining textural and morphological descriptors has been shown to improve the accuracy of biological measurements, in 2D and 3D imaging, particularly in identifying malignant cell types (Kim *et al*., 2010).

In fluorescence microscopy, during acquisition of digital images the intensity value of a pixel is correlated to, but not equal to the number of photons emanating from a corresponding area in the specimen (Berland *et al*., 1998). It is therefore possible to use digital fluorescence microscopy images to extract two types of information: (1) spatial, which can be used to calculate such properties as distances, areas, and velocities; and (2) intensity, which can be used to determine the local concentration of fluorophores in a specimen (Waters, 2009). This technique is frequently employed to assess the relative intensities of specific molecules (Worth and Parsons, 2010), intracellular ion concentrations (Takahashi *et al*., 1999) and the permeability of cell membranes (Zelenina and Brismar, 2000).

3. Difficulties in shape analysis

When performing morphometric analysis, sources of error and accuracy should always be ascertained and, if possible, corrected for. The difficulties encountered by quantitative morphology, as well as reasons for variability, are elaborated in this section.

3.1. Sample processing

To acquire images of sufficient quality, it is essential to use appropriate sample preparation techniques. Shape quantification of biological samples can be static, involving cell fixation, or dynamic, with live cells (Lepekhin *et al*., 2001). The key for cell morphological analyses will greatly depend on good image acquisition, which is directly dependent on sample preparation, the staining performed, and the acquisition methodology (True, 1996). Cell staining protocols for conventional techniques and conditions are easily available. However, complications arise when the cells are presented in unique environments that interfere with the cell staining. Flow of intracellular and extracellular fluids, chemical interactions with fixative reagents (Walker *et al*., 2003), processing time, temperature or pH changes, and excessive staining can affect cellular shape during sample preparation, causing it to differ from the actual *in vivo* scenario. A recent study by Elizondo *et al*. (2012) studied the influence of the preparation route on the supramolecular organization of lipids in a vesicular system. Specifically, marked changes in vesicle composition and homogenization were noted. Thus, fixation protocols, permeabilization, contrast agents and fluorescent labelling approaches and should be carefully chosen and optimized for the specific research objective so as to obtain clean, high-resolution images for processing. Sample preparation methods and imaging techniques are discussed in depth for scanning electron (Goldberg, 2008; Moradi and Behjati, 2012), atomic force (El Kirat *et al*., 2005), and fluorescent microscopy (Hanrahan *et al*., 2011).

3.2. Image analysis

Although image analysis algorithms have evolved immensely over the past decade, shortcomings still exist in detection, isolation, and automated analysis. One of the key processes in accurate image analysis is efficient identification and segmentation of the object(s) of study and reliable measurements of shape descriptors (Chen *et al*., 2012).

Segmentation algorithms are frequently problematic when identifying the outlines of complex shapes and under-segmentation can occur in the instance of multiple cells overlapping (Huan and Lai, 2012). Conversely, over-segmentation can occur if a single cell is subdivided into more than one object and poor contrast between the region of interest and the background can yield unreliable quantification results, which can also compounded by uneven fluorescence detection across the field of view. Segmentation is inherently a foreground–background task, that is, no explicit cell segmentation is performed, and rather each pixel is assigned a binary label as being part of either a cellular or a non-cellular region (Zaritsky *et al*., 2013). The high variability in imaging conditions

DOI: 10.1002/term

and cellular area and contour profiles requires robust algorithms that can deal with this imaging diversity in an automatic and accurate manner, and preferably without the need for manual parameter-tuning. Proposed thresholding methodologies are usually conducted and evaluated on in-house benchmarks that are not freely available to the public. Furthermore, these evaluations often compare accuracy with human annotations and rarely with alternative computational methods, hence are not subjected to a thorough comparative assessment of extant methods (Smith *et al.*, 2013; Zaritsky *et al.*, 2013). The challenges of automated intercellular segmentation are depicted in Figure 4.

Scale and spatial resolution should always be taken into account when quantifying cell shape. Certain image descriptors such as eccentricity and fractal dimensions are invariant to scale (Smith *et al.*, 1996). Measurements that are sensitive to scale should be normalized or complemented with measurements that are not affected by scale or magnification. Critically, sufficient sample numbers are required to obtain meaningful results, to minimize variability, and to ensure that different objects within a group are represented (West *et al.*, 1991). This can be judged with the help of statistical analysis to create a systematic sampling strategy (Collan *et al.*, 1987) and a common technique is to consider object homogeneity within a single field of view.

Computational complexity should also be considered and although quantitative morphological methods are usually inexpensive, they can be time-consuming. For example, real-time shape analysis requires high levels of processing capacity to capture a large number of frames at a high resolution. However, high-throughput imaging methods allow researchers to perform large-scale and highly sensitive imaging-based screening and to observe and mechanistically analyse biological events. For example, a recent study by Kong *et al.* (2013) on histological sections of glioblastoma tissues incorporated the analysis of nuclei, data management, and high-performance computation to support translational research involving nuclear morphometry features, molecular data, and clinical outcomes. Importantly, the results of the study demonstrated that specific nuclear morphogenic features carry prognostic significance and associations with transcriptional and genetic classes, highlighting the potential of high-throughput computational image analysis in histopathology as a complementary approach to human-based review and translational research (Kong *et al.*, 2013).

4. Discussion

The vast range of morphological descriptors available in tissue engineering has enabled the translation of microscopy imaging into quantitative data. However, the complexity of multiple parameters frequently leads to an excess of superfluous data (e.g. elongation vs. aspect ratio analysis), which causes difficulties in the selection and interpretation of results (Soltys *et al.*, 2005). Furthermore, because of the immense variability in cell types, cell states or growth conditions it can be challenging to compare different cell types without bias. Extreme caution should also be exercised when comparing results for the same parameter obtained by different methods. Therefore, an ideal choice of descriptors should be extensive enough to have a reliable basis for both diagnosis and cell classification (Donhuijsen *et al.*, 1991; True 1996; Montironi *et al.*, 2000).

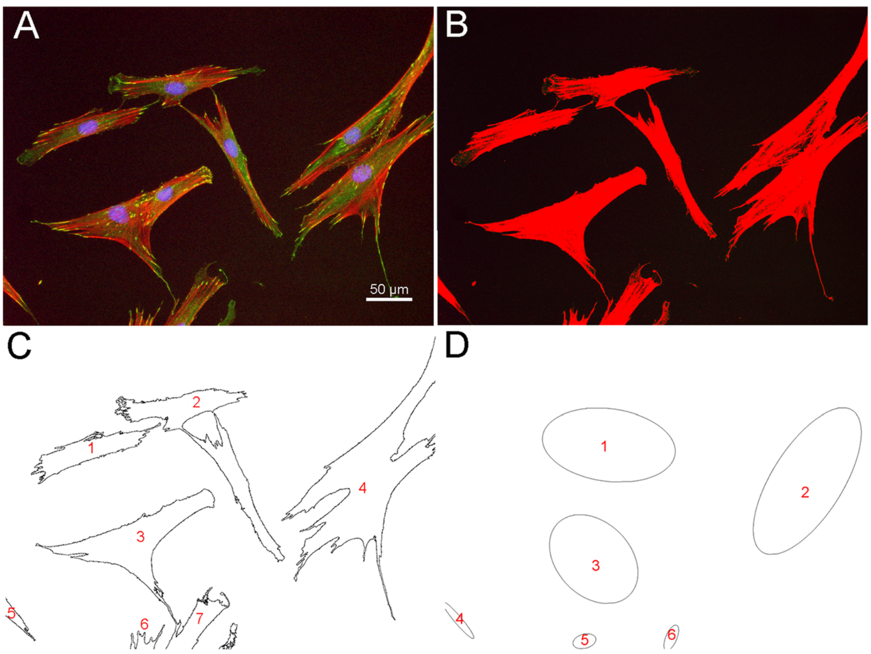

Figure 4. The challenges of automated cellular segmentation. Fluorescently labelled cells (A) are manually thresholded with image analysis software (B). (C,D) Clusters of cells can be grouped into single entities for analysis if cell density is high or if segmentation parameters are not optimized

DOI: 10.1002/term

The assessment of a combination of different parameters introduces new perspectives for the study and avoids redundancy of information; however, it is important to note that morphological analysis must be supported and verified by different experimental approaches (histology, immunohistological and cytochemistry, proteomic, and genomic analysis) to be considered potentially valid and to build a reliable platform for the production of practical applications in a range of tissue types (normal and malignant). In particular, studies assessing tissue engineered constructs must analyse multiple biological and physico-mechanical parameters to identify and verify viable approaches to tissue regeneration and may benefit from multiple and diverse morphological analysis tools and descriptors.

Recently, correlative microscopy has come to the forefront of quantitative imaging as a powerful approach to cellular morphometric analysis through the use of multiple microscopy techniques to characterize a common region of interest. By exploiting advanced sample-preparation, relocation approaches (Brown *et al*., 2009; Mcdonald, 2009), as well as modern labelling approaches that can highlight the structures of interest on multiple microscopy platforms (Ellis, 2008; van Driel *et al*., 2009), such cross-correlative imaging opens up new directions in correlative cell morphometrics (Caplan *et al*., 2011; Jahn *et al*., 2012).

By way of example, a study by Doak *et al*. (2008) recently described the development, evaluation and application of an efficient sample preparation methodology to facilitate coupled atomic force microscopy and confocal laser scanning microscopy (AFM–CLSM), to conduct high-resolution structural and fluorescence imaging. Only through this correlative approach was it possible to demonstrate for the first time that cell filopodia have a 'quilted' surface structure. They also noted that high ultra-structural ridges on the apical cell surface resolved by AFM corresponded to punctate moesin clusters, representing direct visualization of moesin linkages between transmembrane proteins and the cytoskeleton.

Despite the advantages of 3D descriptors in microscopic morphometry, these are not commonly used for characterization studies because of the computational complexity of their measurements. However, several recent studies have confirmed that 3D descriptors seem to be more reliable than quantitative analysis based only on 2D parameters (Meyer *et al*., 2009). For example, nuclear volume, surface area, and sphericity have been considered closer to ideal for grading renal cell carcinomas, improving on both the reproducibility and accuracy obtainable with their 2D counterparts (Choi and Choi, 2007). Recently, 3D electron microscopy has become a powerful tool in structural cell biology as it enables the analysis of subcellular architecture at an unprecedented level of detail (Xylas *et al*., 2012; Martinez-Sanchez *et al*., 2013). Furthermore 3D fractal analyses have found more significant differences between cell classes (Caserta *et al*., 1995), helping to elucidate subtle morphological characteristics that arise during development (Pantic *et al*., 2013a). In tissue engineering, 3D descriptors are often employed to characterize the morphology of porous scaffolds and to assess tissue cellular infiltration, tissue integration and remodelling (Jones *et al*., 2009; Gould *et al*., 2011). However, as 3D analyses have a pre-eminent potential in present scientific research, certain considerations are necessary when using these tools. Three-dimensional cell visualization not only allows researchers to have a more realistic view of cellular and tissue structure but also gives additional information that is not available in 2D images. When a 3D image is projected onto a 2D plane, one dimension of information is lost. Thus, the shape extracted will always represent only a part of the real object.

An exciting area of study benefiting from morphometric analysis is that of stem cell biology and tissue regeneration, with many recent studies indicating that differential stem cell function and cellular morphology are intimately connected. This is particular true in studies focused on the development of biomimetic materials, whereby transferring a stem cell to a micro-/nano-environment that mimics a biological niche induces stem cell function comparable to a cell native to that niche. Studies into topography (Dalby *et al*., 2007c) rigidity (Engler *et al*., 2006) and mechanical loading have identified these external factors as important regulators of stem cell morphology and differential function. Furthermore, these changes have been related to alterations in packing of chromosome territories within the interphase nucleus (Tsimbouri *et al*., 2014).

As new techniques and descriptors appear, morphological categories and grading systems are continually being defined and redefined. There is heterogeneity of procedures, which creates difficulties in comparing results from similar systems, and, in order to improve comparability and quality of studies, efforts must focus on the standardization of methodologies to assess cell morphology. In particular, standard threshold values should be made available for each type of cell and general values of shape descriptors published to facilitate the comparison of these results for future studies.

Frequently, it is useful to conduct discriminant-function analysis or linear discriminant analysis (LDA) to identify the set of descriptors that better discriminates between the groups studied (Soltys *et al*., 2001). Similarly, principal component analysis (PCA) or cluster analysis can be used to remove redundant information and reduce dimensionality of the descriptors (Soltys *et al*., 2005; Kim *et al*., 2010). Recently, however, it has been shown that PCA provides the finest and most compact choice of descriptors for cell shape analysis (Pincus and Theriot, 2007). Nevertheless PCA does have several limitations, mainly because it is a linear scale-dependent method. Furthermore, statistical analysis for 3D features is associated with greater complexity, therefore, cell morphology studies usually only perform statistical analysis using 2D representations of 3D shapes (Pincus and Theriot, 2007).

DOI: 10.1002/term

Integration of image analysis tools with artificial intelligence techniques will lead to a major improvement in precision, accuracy, and reliability of morphometric analyses. Complex shapes can be better quantified with the help of methodologies such as neural networks, machine learning, fuzzy logic and genetic algorithms (Yang Yu *et al.*, 2011; Babazadeh Khameneh *et al.*, 2012), which can be seen as a step towards fine-tuning an automated processes. Three-dimensional reconstruction and modelling software allow for powerful simulations of cells and tissue to be generated with complex anatomical and biophysical properties and morphometry-based systems have been approved in automated cytology systems while semi-automated and automated computer-assisted image analysers are being routinely used in the scientific community with increasing reliability.

5. Conclusion

While cell shape studies have been constantly evolving, there is still a lack of standardization and consensus in the use of descriptors to assess cell shape. A vast number of quantitative features for morphometric analysis can be found. Despite now being able to provide a robust quantitative structural platform for experimental biology, considerable research remains to be done to improve cell shape quantification. The integration of technology and biology is a powerful tool for scientific studies and future applications within the biomedical engineering domain.

Conflict of interest

The authors declare that there is no conflict of interest.

Acknowledgements

The authors thank Maciek Doczyk for assistance in developing illustrations and Anthony Sloan for assistance in preparation of the manuscript. MB is a Science Foundation Ireland SIRG fellow. The authors also thank the AO Exploratory Research Board and SFI for their financial support under project numbers S-09-7P and 11/SIRG/B2135, respectively.

References

Babazadeh Khameneh N, Arabalibeik H, Salehian P, Setayeshi S. 2012; Abnormal red blood cells detection using adaptive neuro-fuzzy system. *Stud Health Technol Inform* **173**: 30–34.

Baker EL, Lu J, Yu D *et al*. 2010; Cancer cell stiffness: integrated roles of three-dimensional matrix stiffness and transforming potential. *Biophys J* **99**: 2048–2057.

Behnam-Motlagh P, Grankvist K, Henriksson R *et al*. 2000; Response in shape and size of individual p31 cancer cells to cisplatin and ouabain: a computerized image analysis of cell halo characteristics during continuous perfusion. *Cytometry* **40**: 198–208.

Berezin V, Skladchikova G, Bock E. 1997; Evaluation of cell morphology by video recording and computer-assisted image analysis. *Cytometry* **27**: 106–116.

Berland K, Jacobson K, French T. 1998; Electronic cameras for low-light microscopy. *Methods Cell Biol* **56**: 19–44.

Bernard F, Bossu JL, Gaillard S. 2001; Identification of living oligodendrocyte developmental stages by fractal analysis of cell morphology. *J Neurosci Res* **65**: 439–445.

Biggs MJ, Richards RG, Gadegaard N *et al*. 2007a; The effects of nanoscale pits on primary human osteoblast adhesion formation and cellular spreading. *J Mater Sci Mater Med* **18**: 399–404.

Biggs MJ, Richards RG, Gadegaard N *et al*. 2007b; Regulation of implant surface cell adhesion: Characterization and quantification of S-phase primary osteoblast adhesions on biomimetic nanoscale substrates. *J Orthop Res* **25**: 273–282.

Biggs MJ, Richards RG, Gadegaard N *et al*. 2009a; Interactions with nanoscale topography: Adhesion quantification and signal transduction in cells of osteogenic and multipotent lineage. *J Biomed Mater Res A* **91**: 195–208.

Biggs MJ, Richards RG, Gadegaard N *et al*. 2009b; The use of nanoscale topography to modulate the dynamics of adhesion formation in primary osteoblasts and ERK/MAPK signalling in STRO-1+enriched skeletal stem cells. *Biomaterials* **30**: 5094–5103.

Binulal NS, Deepthy M, Selvamurugan N *et al*. 2010; Role of nanofibrous poly (caprolactone) scaffolds in human mesenchymal stem cell attachment and spreading for *in vitro* bone tissue engineering-response to osteogenic regulators, *Tissue Eng Pt A* **16**: 393–404.

Boæovi ZL, Tasi MM, Budimlija ZM. 2000; Fractal dimension of hepatocytes' nuclei in normal liver vs. hepatocellular carcinoma (HCC) in human subjects. *J Comp Neurol* **8**: 47–50.

Bonnet N, Lucas L, Ploton D. 1996; Quantitative imaging in electron and confocal microscopies for applications in biology. *Scanning Microsc* **10**: 85–101.

Booth-Gauthier EA, Du V, Ghibaudo M *et al*. 2013; Hutchinson–Gilford progeria syndrome alters nuclear shape and reduces cell motility in three dimensional model substrates. *Integr Biology (Cambr)* **5**: 569–577.

Bowie JE, Young IT. 1977; An analysis technique for biological shape-II. *Acta Cytol* **21**: 455–464.

Boyce JT, Boyce RW, Gunderson HJ, 2010; Choice of morphometric methods and consequences in the regulatory environment. *Toxicol Pathol* **38**: 1128–1133.

Bray MAP, Adams WJ, Geisse NA *et al*. 2010; Nuclear morphology and deformation in engineered cardiac myocytes and tissues. *Biomaterials* **31**: 5143–5150.

Brown E, Mantell J, Carter D, Tilly G, Verkade P. 2009; Studying intracellular transport using high-pressure freezing and Correlative Light Electron Microscopy, *Semin Cell Dev Biol*, **20**: 910–919.

Caplan J, Niethammer M, Taylor RM 2nd *et al*. 2011; The power of correlative microscopy: multi-modal, multi-scale, multi-dimensional. *Curr Opin Struct Biol* **21**: 686–693.

Caserta F, Eldred WD, Fernandez E *et al*. 1995; Determination of fractal dimension of physiologically characterized neurons in two and three dimensions. *J Neurosci Methods* **56**: 133–144.

Cassidy JW, Roberts JN, Smith CA *et al*. 2014; Osteogenic lineage restriction by osteoprogenitors cultured on nanometric grooved surfaces: the role of focal adhesion maturation. *Acta Biomater* **10**: 651–660.

Chang YJ, Hsu CM, Lin CH *et al*. 2013; Electrical stimulation promotes nerve growth factor-induced neurite outgrowth and signaling. *Biochim Biophys Acta* **1830**: 4130–4136.

Chen CS, Mrksich M, Huang S, Whitesides GM, Ingber DE. 1997; Geometric control of cell life and death. *Science* **276**(5317): 1425–1428.

Chen S, Zhao M, Wu G *et al*. 2012; Recent advances in morphological cell image analysis. *Comput Math Methods Med* DOI: 10.1155/2012/101536

Chen X, Zheng B, Liu H. 2011; Optical and digital microscopic imaging techniques

and applications in pathology. *Anal Cell Pathol (Amst)* **34**: 5–18.
Choi HJ, Choi HK. 2007; Grading of renal cell carcino by 3D morphological analysis of cell nuclei. *Comput Biol Med* **37**: 1334–1341.
Chow KH, Factor RE, Ullman KS. 2012; The nuclear envelope environment and its cancer connections. *Nat Rev Cancer* **12**: 196–209.
Collan Y, Torkkeli T, Kosma VM *et al*. 1987; Sampling in diagnostic morphometry: the influence of variation sources. *Pathol Res Pract* **182**: 401–406.
Costa LDF, Manoel ETM, Faucereau F *et al*. 2002; A shape analysis framework for neuromorphometry. *Network* **13**: 283–310.
Dalby MJ, Biggs MJ, Gadegaard N *et al*. 2007a; Nanotopographical stimulation of mechanotransduction and changes in interphase centromere positioning. *J Cell Biochem* **100**: 326–338.
Dalby MJ, Biggs MJ, Gadegaard N *et al*. 2007b; Nanotopographical stimulation of mechanotransduction and changes in interphase centromere positioning. *J Cell Biochem* **100**: 326–338.
Dalby MJ, Gadegaard N, Tare R *et al*. 2007c; The control of human mesenchymal cell differentiation using nanoscale symmetry and disorder. *Nat Mater* **6**: 997–1003.
Daniel B, DeCoster MA. 2004; Quantification of sPLA2-induced early and late apoptosis changes in neuronal cell cultures using combined TUNEL and DAPI staining. *Brain Res Brain Res Protoc* **13**: 144–150.
Débarre D, Botcherby EJ, Watanabe T *et al*. 2009; Image-based adaptive optics for two-photon microscopy. *Opt Lett* **34**: 2495–2497.
Deister C, Aljabari S, Schmidt CE. 2007; Effects of collagen 1, fibronectin, laminin and hyaluronic acid concentration in multi-component gels on neurite extension. *J Biomat Sci-Polym E* **18**: 983–997.
den Braber ET, de Ruijter JE, Ginsel LA *et al*. 1996; Quantitative analysis of fibroblast morphology on microgrooved surfaces with various groove and ridge dimensions, *Biomaterials* **17**: 2037–2044.
Doak SH, Rogers D, Jones B *et al*. 2008; High-resolution imaging using a novel atomic force microscope and confocal laser scanning microscope hybrid instrument: essential sample preparation aspects. *Histochem Cell Biol* **130**: 909–916.
Donhuijsen K, Schulz S, Leder LD. 1991; Nuclear grading of renal cell carcinomas – is morphometry necessary? *J Cancer Res Clin Oncol* **117**: 73–78.
Einstein AJ, Wu HS, Sanchez M, Gil J. 1998; Fractal characterization of chromatin appearance for diagnosis in breast cytology. *J Pathol* **185**: 366–381.
El Kirat K, Burton I, Dupres V, Dufrene YF. 2005; Sample preparation procedures for biological atomic force microscopy. *J Microsc-Oxford* **218**: 199–207
Eliceiri KW, Berthold MR, Goldberg IG *et al*. 2012; Biological imaging software tools. *Nat Methods* **9**: 697–710.
Elizondo E, Larsen J, Hatzakis NS *et al*. 2012; Influence of the preparation route on the supramolecular organization of lipids in a vesicular system. *J Am Chem Soc* **134**: 1918–1921.
Ellis EA. 2008; Correlative transmission microscopy: cytochemical localization and immunocytochemical localization in studies of oxidative and nitrosative stress. *Methods Mol Biol* **477**: 41–48.
Emde A, Pradeep CR, Ferraro DA *et al*. 2011; Combining epitope-distinct antibodies to HER2: cooperative inhibitory effects on invasive growth. *Oncogene* **30**: 1631–1642.
Engler AJ, Sen S, Sweeney HL, Discher DE. 2006; Matrix elasticity directs stem cell lineage specification, *Cell* **126**: 677–689.
Forgacs G. 1995; On the possible role of cytoskeletal filamentous networks in intracellular signaling – an approach based on percolation. *J Cell Sci* **108**: 2131–2143.
Fujikawa K, Sasaki M, Aoyama T *et al*. 1997; Role of volume weighted mean nuclear volume for predicting disease outcome in patients with renal cell carcinoma. *J Urol* **157**: 1237–1241.
Goldberg MW. 2008; Immunolabeling for scanning electron microscopy (SEM) and field emission SEM. *Methods Cell Biol* **88**: 109–130.
Gould DJ, Vadakkan TJ, Poche RA *et al*. 2011; Multifractal and lacunarity analysis of microvascular morphology and remodeling. *Microcirculation* **18**: 136–151.
Guarino V, Guaccio A, Netti PA *et al*. 2010; Image processing and fractal box counting: User-assisted method for multi-scale porous scaffold characterization. *J Mater Sci Mater M* **21**: 3109–3118.
Hanrahan O, Harris J, Egan C. 2011; Advanced microscopy: laser scanning confocal microscopy. *Methods Mol Biol* **784**: 169–180
Heiberg KH, Kemp J. 1929; Ueber die zahl der chromosomen in carcinomzellen bein menschen, *Virch Arch* **273**: 693–700.
Helmy IM, Azim AM. 2012; Efficacy of ImageJ in the assessment of apoptosis. *Diagn Pathol* **7**(15). DOI: 10.1186/1746-1596-7-15
Hevia D, Mayo JC, Quiros I *et al*. 2010; Monitoring intracellular melatonin levels in human prostate normal and cancer cells by HPLC. *Anal Bioanal Chem* **397**: 1235–1244.
Hevia D, Rodriguez-Garcia A, Alonso-Gervós M *et al*. 2011; Cell volume and geometric parameters determination in living cells using confocal microscopy and 3D reconstruction. *Protocol Exchange*. doi: 10.1038/protex.2011.272.
Hines ML, Carnevale NT. 2001; NEURON: a tool for neuroscientists. *Neuroscientist* **7**: 123–135.
Howard L, Wyatt S, Nagappan G *et al*. 2013; Prongf promotes neurite growth from a subset of ngf-dependent neurons by a p75ntr-dependent mechanism. *Development* **140**: 2108–2117.
Huan PW, Lai YH. 2012; Effective segmentation and classification for HCC biopsy images. *Pattern Recogn* **43**: 1550–1563.
Jacob W. 1925; Uber das rhythmische wachstum der zellen durch verdopplung ihres volumens. *Roux Archiv Entwicklungs Mechanik* **106**: 124–192.
Jahn KA, Barton DA, Kobayashi K *et al*. 2012; Correlative microscopy: providing new understanding in the biomedical and plant sciences. *Micron* **43**: 565–582.
Jiang H, Zhu WJ, Li J *et al*. 2014; Quantitative histological analysis and ultrastructure of the aging human testis. *Int Urol Nephrol* **46**: 879–885.
Jones AC, Arns CH, Hutmacher DW *et al*. 2009; The correlation of pore morphology, interconnectivity and physical properties of 3D ceramic scaffolds with bone ingrowth. *Biomaterials* **30**: 1440–1451.
Kantawong F, Burgess KE, Jayawardena K *et al*. 2009; Whole proteome analysis of osteoprogenitor differentiation induced by disordered nanotopography and mediated by erk signalling. *Biomaterials* **30**: 4723–4731.
Kawa A, Stahlhut M, Berezin A *et al*. 1998; A simple procedure for morphometric analysis of processes and growth cones of neurons in culture using parameters derived from the contour and convex hull of the object. *J Neurosci Methods* **79**: 53–64.
Keren K, Pincus Z, Allen GM *et al*. 2008; Mechanism of shape determination in motile cells. *Nature* **453**: 475–480.
Khoshfetrat AB, Kino-Oka M, Takezawa Y *et al*. 2008; Effect of transforming growth factor-beta1 on morphological characteristics relating to migration and differentiation of rabbit chondrocytes cultured in collagen gels. *J Biosci Bioeng* **106**: 547–553.
Kiehl TR, Shen D, Khattak SF *et al*. 2011; Observations of cell size dynamics under osmotic stress. *Cytometry Part A J Int Soc Anal Cytol* **79**: 560–569.
Kim MH, Tsubakino N, Kagita S *et al*. 2011; Characterization of spatial cell distribution in multilayer sheet of human keratinocytes through a stereoscopic cell imaging system. *J Biosci Bioeng* **112**: 289–291.
Kim TY, Choi HJ, Hwang HG *et al*. 2010; Three-dimensional texture analysis of renal cell carcinoma cell nuclei for computerized automatic grading. *J Med Syst* **34**: 709–716.
Kong J, Wasng F, Teodoro G *et al*. 2013; High-Performance Computational Analysis Of Glioblastoma Pathology Images With Database Support Identifies Molecular and Survival Correlates. Proceedings, IEEE International Conference on Bioinformatics and Biomedicine; 229–236.
Kothapalli CR, Kamm RD. 2013; 3D matrix microenvironment for targeted differentiation of embryonic stem cells into neural and glial lineages. *Biomaterials* **34**: 5995–6007.
Kraskiewicz H, Breen B, Sargeant T, McMahon S, Pandit A. 2013; Assembly of protein-based hollow spheres encapsulating a therapeutic factor. *ACS Chem Neurosci* **4**: 1297–1304.
Kumar G, Tison CK, Chatterjee K *et al*. 2011; The determination of stem cell fate by 3D scaffold structures through the control of cell shape. *Biomaterials* **32**: 9188–9196.
Lang S, Muller B, Dominietto MD *et al*. 2012; Three-dimensional quantification of capillary networks in healthy and cancerous tissues of two mice. *Microvasc Res* **84**: 314–322.
Lautscham LA, Lin CY, Auernheimer V *et al*. 2014; Biomembrane-mimicking lipid bilayer system as a mechanically tunable cell substrate. *Biomaterials* **35**: 3198–3207.
Lepekhin EA, Walmod PS, Berezin A *et al*. 2001; Evaluation of cell morphology. *Methods Mol Biol* **161**: 85–100.
Leslie-Barbick JE, Saik JE, Gould DJ *et al*. 2011; The promotion of microvasculature formation in poly(ethylene glycol) diacrylate hydrogels by an immobilized vegf-mimetic peptide. *Biomaterials* **32**: 5782–5789.

Liautaud-Roger F, Teyssier JR, Ferre D *et al*. 1992; Can chromatin texture predict structural karyotypic changes in diploid cells from thyroid cold nodules? *Anal Cell Pathol* **4**: 421–428.
Liu X, Zhang X, Lee I. 2010; A quantitative study on morphological responses of osteoblastic cells to fluid shear stress. *Acta biochimica et biophysica Sinica* **42**(3): 195–201.
Liu X, Zhang X, Lee I. 2010; A quantitative study on morphological responses of osteoblastic cells to fluid shear stress. *Acta Biochimica et Biophysica Sinica* **42**(3): 195–201.
Lopez DJ, Egido-Gabas M, Lopez-Montero I *et al*. 2012; Accumulated bending energy elicits neutral sphingomyelinase activity in human red blood cells. *Biophys J* **102**: 2077–2085.
Losa GA. 2012; Fractals and their contribution to biology and medicine. *Medicographia* **34**: 365–374.
Losa GA, Castelli C. 2005; Nuclear patterns of human breast cancer cells during apoptosis: characterization by fractal dimension and co-occurrence matrix statistics. *Cell Tissue Res* **322**: 257–267.
Losa GA, Graber R, Baumann G *et al*. 1998; Steroid hormones modify nuclear heterochromatin structure and plasma membrane enzyme of MCF-7 cells. A combined fractal, electron microscopical and enzymatic analysis. *Eur J Histochem* **42**: 21–29.
Luzzati F, Fasolo A, Peretto P. 2011; Combining confocal laser scanning microscopy with serial section reconstruction in the study of adult neurogenesis. *Front Neurosci* **5**: doi: 10.3389/fnins.2011.00070
Mandelbrot BB, 1982; *The fractal geometry of nature*, W. H. Freeman and Company: New York.
Martinez-Sanchez A, Garcia I, Fernandez JJ. 2013; A ridge-based framework for segmentation of 3D electron microscopy datasets. *J Struct Biol* **181**: 61–70.
Massia SP, Hubbell JA. 1991; Human endothelial-cell interactions with surface-coupled adhesion peptides on a nonadhesive glass substrate and 2 polymeric biomaterials. *J Biomed Materials Res* **25**: 223–242.
Mauri A, Zeisberger SM, Hoerstrup SP *et al*. 2013; Analysis of the uniaxial and multiaxial mechanical response of a tissue-engineered vascular graft. *Tissue Eng A* **19**: 583–592.
Mcdonald KL. 2009; A review of high-pressure freezing preparation techniques for correlative light and electron microscopy of the same cells and tissues. *J Microsc Oxf* **235**: 273–281
McKee CT, Wood JA, Ly I *et al*. 2012; The influence of a biologically relevant substratum topography on human aortic and umbilical vein endothelial cells. *Biophys J* **102**: 1224–1233.
Metzler V, Bienert H, Lehmann T *et al*. 1999; A novel method for quantifying shape deformation applied to biocompatibility testing. *ASAIO J* **45**: 264–271.
Metzler V, Lehmann T, Bienert H *et al*. 2000; Scale-independent shape analysis for quantitative cytology using mathematical morphology. *Comput Biol Med* **30**: 135–151.
Meyer MG, Fauver M, Rahn JR *et al*. 2009; Automated cell analysis in 2D and 3D: a comparative study. *Pattern Recogn* **42**: 141–146.
Montironi R, Santinelli A, Pomante R *et al*. 2000; Morphometric index of adult renal cell carcinoma. Comparison with the Fuhrman grading system. *Virchows Arch* **437**: 82–89.
Moradi I, Behjati M. 2012; Six common errors cause dangerous mistakes in interpretation of electron micrographs. *Microsc Res Tech* **75**: 677–682.
Moustakas A, Stournaras C. 1999; Regulation of actin organisation by TGF-beta in H-ras-transformed fibroblasts. *J Cell Sci* **112**: 1169–1179.
Muller P, Langenbach A, Kaminski A *et al*. 2013; Modulating the actin cytoskeleton affects mechanically induced signal transduction and differentiation in mesenchymal stem cells. *PLoS One* **8**: e71283. DOI: 10.1371/journal.pone.0071283
Muniandy SV, Stanslas J. 2008; Modelling of chromatin morphologies in breast cancer cells undergoing apoptosis using generalized Cauchy field. *Comput Med Imag Graph* **32**: 631–637.
Nafe R, Glienke W, Schlote W *et al*. 2001; EGFR gene amplification in glioblastomas. Is there a relationship with morphology of tumor cell nuclei and proliferative activity? *Anal Quant Cytol Histol* **23**: 135–143.
Nandakumar V, Kelbauskas L, Johnson R *et al*. 2011; Quantitative characterization of preneoplastic progression using single-cell computed tomography and three-dimensional karyometry. *Cytometry A* **79**: 25–34.
Nandakumar V, Kelbauskas L, Hernandez KF *et al*. 2012; Isotropic 3D nuclear morphometry of normal, fibrocystic and malignant breast epithelial cells reveals new structural alterations. *PLoS One* **7**: e29230. DOI: 10.1371/journal.pone.0029230
Nativ O, Sabo E, Raviv G *et al*. 1995; The role of nuclear morphometry for predicting disease outcome in patients with localized renal cell carcinoma. *Cancer* **76**: 1440–1444.
Nayar AK, Sundharam BS. 2003; Cytomorphometric analysis of exfoliated normal buccal mucosa cells. *Indian J Dent Res* **14**: 87–93.
Nagashima T, Suzuki M, Oshida M, Hishimoto H, Yagata H, Shishikura T, Koda K, Nakajima N. 1998; Morphometry in the cytologic evaluation of thyroid follicular lesions. *Cancer* **84**(2): 115–118.
Ntziachristos V. 2010; Going deeper than microscopy: the optical imaging frontier in biology. *Nat Methods* **7**: 603–614.
Oh HH, Ko YG, Uyama H *et al*. 2014; Fabrication and characterization of thermoresponsive polystyrene nanofibrous mats for cultured cell recovery. *BioMed Res Int* 480694: doi: 10.1155/2014/480694.
Oh S, Brammer KS, Li YS *et al*. 2009; Stem cell fate dictated solely by altered nanotube dimension. *Proc Natl Acad Sci U S A* **106**: 2130–2135.
Ohri S, Dey P, Nijhawan R. 2004; Fractal dimension in aspiration cytology smears of breast and cervical lesions. *Anal Quant Cytol* **26**: 109–112.
Pantic I, Basta-Jovanovic G, Starcevic V *et al*. 2013a; Complexity reduction of chromatin architecture in macula densa cells during mouse postnatal development. *Nephrology* **18**: 117–124.
Pantic I, Pantic S, Paunovic J *et al*. 2013b; Nuclear entropy, angular second moment, variance and texture correlation of thymus cortical and medullar lymphocytes: grey level co-occurrence matrix analysis. *Ann Acad Bras Cienc* **85**: 1063–1072.
Pantic I, Paunovic J, Perovic M. 2013c; Time-dependent reduction of structural complexity of the buccal epithelial cell nuclei after treatment with silver nanoparticles. *J Microsc* **252**: 286–294.
Pasqualato A, Palombo A, Cucina A *et al*. 2012; Quantitative shape analysis of chemoresistant colon cancer cells: correlation between morphotype and phenotype. *Exp Cell Res* **318**: 835–846.
Payne CM, Bjore CG, Cromey DW, Roland F. 1989; A comparative mathematical evaluation of contour irregularity using form factor and PERBAS, a new analytical shape factor. *Anal Quant Cytol Histol* **11**: 341–352.
Payne M, Wang D, Sinclair CM *et al*. 2014; Automated quantification of neurite outgrowth orientation distributions on patterned surfaces, *J Neur Eng* **11**: 046006. DOI: 10.1088/1741-2560/11/4/046006
Pearson EC. 1986; Correlations between nuclear morphology and bundles of cytoplasmic fibrils in 50 cases of acute myeloid-leukemia. *J Clin Pathol* **39**: 99–104.
Pincus Z, Theriot JA. 2007; Comparison of quantitative methods for cell-shape analysis. *J Microsc* **227**: 140–156.
Rayatpisheh S, Heath DE, Shakouri A *et al*. 2014; Combining cell sheet technology and electrospun scaffolding for engineered tubular, aligned, and contractile blood vessels. *Biomaterials* **35**: 2713–2719.
Rocchi MBL, Sisti D, Albertini MC *et al*. 2007; Current trends in shape and texture analysis in neurology: aspects of the morphological substrate of volume and wiring transmission. *Brain Res Rev* **55**: 97–107.
Roskelley CD, Desprez PY, Bissell MJ. 1994; Extracellular matrix-dependent tissue-specific gene expression in mammary epithelial cells requires both physical and biochemical signal transduction. *Proc Natl Acad Sci U S A* **91**: 12378–12382.
Royo-Gascon N, Wininger M, Scheinbeim JI *et al*. 2013; Piezoelectric substrates promote neurite growth in rat spinal cord neurons. *Ann Biomed Eng* **41**: 112–122.
Sackmann E. 1994; Membrane bending energy concept of vesicle-shape and cell-shape and shape-transitions. *Febs Lett* **346**: 3–16.
Satyam A, Kumar P, Fan X, Gorelov A, Rochev Y, Joshi L, Lyden D, Thomas B, Rodriguez B, Raghunath M, Pandit A, Zeugolis D. 2014; Macromolecular crowding meets tissue engineering by self-assembly: A paradigm shift in regenerative medicine. *Adv Mater* **346**(19): 3024–3034.
Schiller HB, Fassler R. 2013; Mechanosensitivity and compositional dynamics of cell-matrix adhesions. *EMBO Rep* **14**: 509–519.
Schneider CA, Rasband WS, Eliceiri KW. 2012; NIH Image to ImageJ: 25 years of image analysis. *Nat Methods* **9**: 671–675.
Sheets KG, Jun B, Zhou Y *et al*. 2013; Microglial ramification and redistribution concomitant with the attenuation of choroidal neovascularization by neuroprotectin D1. *Mol Vision* **19**: 1747–1759.

Smith R, Ventura D, Prince JT. 2013; Novel algorithms and the benefits of comparative validation. *Bioinformatics* **29**: 1583–1585.
Smith TG, Lange GD, Marks WB. 1996; Fractal methods and results in cellular morphology – dimensions, lacunarity and multifractals. *J Neurosci Methods* **69**: 123–136.
Soll DR, Voss E, Varnum-Finney B *et al*. 1988; 'Dynamic Morphology System': a method for quantitating changes in shape, pseudopod formation, and motion in normal and mutant amoebae of *Dictyostelium discoideum*. *J Cell Biochem* **37**: 177–192.
Soltys Z, Ziaja M, Pawlínski R *et al*. 2001; Morphology of reactive microglia in the injured cerebral cortex. Fractal analysis and complementary quantitative methods. *J Neurosci Res* **63**: 90–97
Soltys Z, Orzylowska-Sliwinska O, Zaremba M *et al*. 2005; Quantitative morphological study of microglial cells in the ischemic rat brain using principal component analysis. *J Neurosci Methods* **146**: 50–60.
Song W, Liu W, Niu X *et al*. 2013; Three-dimensional morphometric comparison of normal and apoptotic endothelial cells based on laser scanning confocal microscopy observation. *Microsc Res Tech* **76**: 1154–1162.
Spillane M, Ketschek A, Donnelly CJ *et al*. 2012; Nerve growth factor-induced formation of axonal filopodia and collateral branches involves the intra-axonal synthesis of regulators of the actin-nucleating arp2/3 complex. *J Neurosci* **32**: 17671–17689.
Stahlhut M, Berezin V, Bock E *et al*. 1997; NCAM-fibronectin-type-III-domain substrata with and without a six-amino-acid-long proline-rich insert increase the dendritic and axonal arborization of spinal motoneurons. *J Neurosci Res* **48**: 112–121.
Takahashi A, Camacho P, Lechleiter JD *et al*. 1999; Measurement of intracellular calcium. *Physiol Rev* **79**: 1089–1125
Thurner P, Müller R, Raeber G *et al*. 2005; 3D morphology of cell cultures: a quantitative approach using micrometer synchrotron light tomography. *Microsc Res Tech* **66**: 289–298.
Tong WY, Shen W, Yeung CW *et al*. 2012; Functional replication of the tendon tissue microenvironment by a bioimprinted substrate and the support of tenocytic differentiation of mesenchymal stem cells. *Biomaterials* **33**: 7686–7698.
True LD. 1996; Morphometric applications in anatomic pathology. *Hum Pathol* **27**: 450–467.
Tsimbouri P, Gadegaard N, Burgess K *et al*. 2014; Nanotopographical effects on mesenchymal stem cell morphology and phenotype. *J Cell Biochem* **115**: 380–390.
van Driel LF, Valentijn JA, Valentijn KM *et al*. 2009; Tools for correlative cryo-fluorescence microscopy and cryo-electron tomography applied to whole mitochondria in human endothelial cells. *Eur J Cell Biol* **88**: 669–684.
van Pelt J, Schierwagen A. 2004; Morphological analysis and modeling of neuronal dendrites. *Math Biosci* **188**: 147–155.
van Velthoven R, Petein M, Oosterlinck WJ *et al*. 1995; The use of digital image analysis of chromatin texture in Feulgen-stained nuclei to predict recurrence of low grade superficial transitional cell carcinoma of the bladder. *Cancer* **75**: 560–568.
Walker DC, Brown BH, Blackett AD *et al*. 2003; A study of the morphological parameters of cervical squamous epithelium. *Physiol Meas* **24**: 121–135.
Wan LQ, Kang SM, Eng G *et al*. 2010; Geometric control of human stem cell morphology and differentiation. *Integr Biol* **2**: 346–353.
Waters JC. 2009; Accuracy and precision in quantitative fluorescence microscopy. *J Cell Biol* **185**: 1135–1148.
Watson PA. 1991; Function follows form: generation of intracellular signals by cell deformation. *FASEB J* **5**: 2013–2019.
Watt FM, Jordan PW, O'Neill CH. 1988; Cell shape controls terminal differentiation of human epidermal keratinocytes. *Proc Natl Acad Sci U S A* **85**: 5576–5580.
West MJ, Slomianka L, Gundersen HJ. 1991; Unbiased stereological estimation of the total number of neurons in thesubdivisions of the rat hippocampus using the optical fractionator. *Anat Rec* **231**: 482–497.
Wood MD, Willits RK. 2009; Applied electric field enhances drg neurite growth: influence of stimulation media, surface coating and growth supplements. *J Neur Eng* **6**: 1741–2560.
Worth DC, Parsons M. 2010; Advances in imaging cell-matrix adhesions. *J Cell Sci* **123**: 3629–3638.
Wu QF, Yang L, Li S *et al*. 2012; Fibroblast growth factor 13 is a microtubule-stabilizing protein regulating neuronal polarization and migration. *Cell* **149**: 1549–1564.
Xiong Y, Iglesias PA. 2010; Tools for analyzing cell shape changes during chemotaxis. *Integr Biol* **2**: 561–567.
Xylas J, Quinn KP, Hunter M, Georgakoudi I. 2012; Improved fourier-based characterization of intracellular fractal features. *Opt Express* **20**: 23442–23455.
Yang Yu B, Elbuken C, Ren CL *et al*. 2011; Image processing and classification algorithm for yeast cell morphology in a microfluidic chip. *J Biomed Opt* **16**: 066008; DOI: 10.1117/1.3589100
Yao L, Wang S, Cui W *et al*. 2009; Effect of functionalized micropatterned PLGA on guided neurite growth. *Acta Biomater* **5**: 580–588.
Zaritsky A, Manor N, Wolf L *et al*. 2013; Benchmark for multi-cellular segmentation of bright field microscopy images. *BMC Bioinformatics* **14**: 319.
Zelenina M, Brismar H. 2000; Osmotic water permeability measurements using confocal laser scanning microscopy. *Eur Biophys J Biophy* **29**: 165–171.
Zhang D, Lu G. 2004; Review of shape representation and description techniques. *Pattern Recogn* **37**: 1–19.
Zychowicz M, Mehn D, Ruiz A *et al*. 2012; Patterning of human cord blood-derived stem cells on single cell posts and lines: implications for neural commitment. *Acta Neurobiol Exp* **72**: 325–336.